

Updated Results of a Solid-State Sensor Irradiation Study for ILC Extreme Forward Calorimetry

Talk presented at the International Workshop on Future Linear Colliders (LCWS15), Whistler, Canada, 2-6 November 2015.

George Courcoubetis, Wyatt Crockett, Vitaliy Fadeyev, Caleb Fink, Nikolas Guillemaud, Cesar Gonzalez Renteria, Benjamin Gruey, Patrick LaBarre, Forest Martinez-McKinney, Greg Rischbieter, Bruce A. Schumm*, Edwin Spencer, Max Wilder

Santa Cruz Institute for Particle Physics and the University Of California, 1156 High Street, Santa Cruz, California 95064 USA

Abstract

Detectors proposed for the International Linear Collider (ILC) incorporate a tungsten sampling calorimeter ('Beam-Cal') intended to reconstruct showers of electrons, positrons and photons that emerge from the interaction point of the collider with angles between 5 and 50 milliradians. For the innermost radius of this calorimeter, radiation doses at shower max are expected to reach 100 Mrad per year, primarily due to minimum-ionizing electrons and positrons that arise in the induced electromagnetic showers of e^+e^- 'beamstrahlung' pairs produced in the ILC beam-beam interaction. However, radiation damage to calorimeter sensors may be dominated by hadrons induced by nuclear interactions of shower photons, which are much more likely to contribute to the non-ionizing energy loss that has been observed to damage sensors exposed to hadronic radiation. We report here on the results of SLAC Experiment T-506, for which several different types of silicon diode and gallium-arsenide sensors were exposed to doses of radiation induced by showering electrons of energy 3.5-13.3 GeV. By embedding the sensor under irradiation within a tungsten radiator, the exposure incorporated hadronic species that would potentially contribute to the degradation of a sensor mounted in a precision sampling calorimeter. Depending on sensor technology, efficient charge collection was observed for doses as large as 270 Mrad.

Keywords:

Semiconductor sensors, Radiation damage, ILC Beamline Calorimeter

1. Introduction

Far-forward calorimetry, covering the region between 5 and 50 milliradians from the on-energy beam axis, is envisioned as a component of both the ILD [2] and SiD [3] detector concepts for the proposed International Linear Collider (ILC). The BeamCal tungsten sampling

calorimeter proposed to cover this angular region is expected to absorb approximately 10 TeV of electromagnetic radiation per beam crossing from e^+e^- beamstrahlung pairs, leading to expected annual radiation doses of 100 Mrad for the most heavily-irradiated portions of the instrument. While the deposited energy is expected to arise primarily from minimum-ionizing electrons and positrons in the induced electromagnetic showers, radiation damage to calorimeter sensors may be dominated by hadrons induced by nuclear interac-

*Corresponding author.

Email address: baschumm@ucsc.edu (Bruce A. Schumm)

tions of shower photons, which are much more likely to contribute to the non-ionizing energy loss that has been observed to damage sensors exposed to hadronic radiation. We report here on the latest results of SLAC Experiment T-506, for which several different types of silicon diode and gallium-arsenide (GaAs) sensors were exposed to doses of up to 270 Mrad at the approximate maxima of electromagnetic showers induced in a tungsten radiator by electrons of energy 3.5-13.3 GeV, similar to that of electrons and positrons from ILC beamstrahlung pairs.

Bulk damage leading to the suppression of the electron/hole charge-collection efficiency (CCE) is generally thought to be proportional to the non-ionizing energy loss ('NIEL') component of the energy deposited by the incident radiation. Early studies of electromagnetically-induced damage to solar cells [4, 5, 6] suggested that p-type bulk sensors were more tolerant to damage from electromagnetic sources, due to an apparent departure from NIEL scaling, particularly for electromagnetic particles of lower incident energy.

Several more-recent studies have explored radiation tolerance of silicon diode to incident fluxes of electrons. A study assessing the capacitance vs. bias voltage (CV) characteristics of sensors exposed to as much as 1 Grad of incident 2 MeV electrons [7] suggested approximately 35 times less damage to n-type magnetic Czochralski sensors than that expected from NIEL scaling. A study of various n-type sensor types exposed to 900 MeV electrons showed charge-collection loss of as little as 3% for exposures up to 50 Mrad exposure [8]; for exposures of 150 Mrad, a suppression of damage relative to NIEL expectations of up to a factor of four was observed [9]. These discrepancies have been attributed to the different types of defects created by lattice interactions: electrons tend to create point-like defects that are more benign than the clusters formed due to hadronic interactions.

Finally, in studies of sensors exposed to large doses of hadron-induced radiation, p-type bulk silicon was found to be more radiation-tolerant than n-type bulk silicon, an observation that has been attributed to the absence of type inversion and the collection of an electron-based signal [10, 11]. However, n-type bulk devices have certain advantages, such as a natural inter-electrode isolation with commonly used passivation materials such as silicon oxide and silicon nitride.

More recently, GaAs sensors have been proposed as a possible radiation-tolerant alternative to silicon sensors, the latter of which can develop large dark current after significant irradiation. GaAs sensors, on the other hand, have been observed [12] to suffer significant loss

of CCE for moderate doses of 10-MeV-scale electrons.

Here, we report on an exploration of the radiation tolerance of silicon and GaAs sensors, assessed via direct measurements of the median collected charge deposited by minimum-ionizing particles. For some of the sensors, leakage current measurement were also made. Four different silicon-diode bulk compositions were explored: p-type and n-type doping of both magnetic Czochralski and float-zone crystals. Both strip and pad geometries were explored, depending on which sensor samples were available. For strip sensors, p-type float-zone sensors were produced by Hamamatsu Photonics while the remaining types were produced by Micron Corporation. Sensor strip pitch varied between 50 and 100 μm , while the bulk thickness varied between 307 μm (for the p-type magnetic Czochralski sensors) and 320 μm (for the p-type float zone sensors). A p-type float-zone pad sensor (part number WSI-P4), 320 μm thick and manufactured as a test structure on the same wafer as ATLAS upgrade prototype sensors [1], was also exposed and studied. Also explored was the radiation tolerance of 300 μm -thick GaAs pad sensors produced by means of the Liquid Encapsulated Czochralski method doped by a shallow donor (Sn or Te; Sn was used for the sensor in this study) [12]. Relative to a prior report [13] on the radiation tolerance of silicon diode sensors, this report includes new results on a 270 Mrad exposure and annealing study of the WSI-P4 p-type bulk float-zone silicon diode pad sensor, as well as new results based on a recent run of experiment T-506 in which GaAs pad sensors was exposed to doses of 5.7 and 20.8 Mrad.

While the radiation dose was initiated by electromagnetic processes (electrons showering in tungsten), the placement of the sensors near shower max ensures that the shower incorporates an appropriate component of hadronic irradiation arising from neutron spallation, photoproduction, and the excitation of the Δ resonance. Particularly for the case that NIEL scaling suppresses electromagnetically-induced radiation damage, the small hadronic component of the electromagnetic shower might dominate the rate of damage to the sensor. However, the size and effect of this component is difficult to estimate reliably, and so we choose to study radiation damage in a configuration that naturally incorporates all components present in an electromagnetic shower.

2. Experimental Setup

Un-irradiated sensors were subjected to current vs. bias voltage (IV) and capacitance vs. bias voltage

(CV) tests, the results of which allowed a subset of them to be selected for irradiation based on their breakdown voltage (typically above 1000 V for selected sensors) and low level of leakage current. The sensors were placed on carrier printed-circuit ‘daughter boards’ and wire-bonded to a readout connector. The material of the daughter boards was milled away in the region to be irradiated in order to facilitate the charge collection measurement (described below) and minimize radio-activation. The median collected charge was measured with the Santa Cruz Institute for Particle Physics (SCIPP) charge-collection (CC) apparatus (also described below) before irradiation. The sensors remained mounted to their individual daughter boards throughout irradiation and the followup tests, simplifying their handling and reducing uncontrolled annealing. Additionally, this allowed a reverse-bias voltage to be maintained across the sensor during irradiation. This voltage was kept small (at the level of a few volts) to avoid possible damage of the devices from a large instantaneous charge during the spill.

Sensors were irradiated with beam provided by the End Station Test Beam (ESTB) facility at the SLAC National Accelerator Laboratory. Parameters of the beam provided by the ESTB facility are shown in Tab. 1. The beam was incident upon a series of tungsten radiators. An initial 7mm-thick (2.0 radiation-length) tungsten plate (‘R1’) served to initiate the electromagnetic shower. The small number of radiation lengths of this initial radiator permitted the development of a small amount of divergence of the shower relative to the straight-ahead beam direction without significant development of the largely isotropic hadronic component of the shower.

Table 1: Parameters of the beam delivered by the ESTB facility during the T-506 experiment.

Parameter	Value
Energy	3.5-13.3 GeV
Repetition Rate	5-10 Hz
Charge per Pulse	150-180 pC
Spot Size (radius)	~ 1 mm

This plate was followed by an open length of approximately half a meter, which allowed a degree of spreading of the shower before it impinged upon a second, significantly thicker ‘R2’ (4.0 radiation-length) tungsten plate, which was followed immediately by the sensor undergoing irradiation. This was closely followed, in turn, by an 8.0 radiation-length tungsten plate. Immedi-

ately surrounding the sensor by tungsten radiators that both initiated and absorbed the great majority of the electromagnetic shower ensured that the sensor would be illuminated by a flux of hadrons commensurate with that experienced by a calorimeter sensor close to the maximum of a tungsten-induced shower. More precise values of the location of the various radiator elements and sensor, for each of the three years of running of T-506, are given in Tab. 2.

Table 2: Location of the various radiator elements and the sensor under irradiation, for the three successive phases of T-506 running. The R1 radiator had a thickness of $2 X_0$, while the thickness of the R2 radiator was $4 X_0$. The apparent increased geometrical thickness of R2 in Year 1 was due to the presence of a 6mm air gap mid-way through the radiator.

Surface	Year 1	Year 2	Year 3
	(2013)	(2014)	(2015)
	Location	Location	Location
	(cm)	(cm)	(cm)
R1 Entrance	0.0	0.0	0.0
R1 Exit	0.7	0.7	0.7
R2 Entrance	55.0	45.7	46.6
R2 Exit	57.0	47.1	48.0
Sensor	57.7	47.6	48.5

Although initiating the shower significantly upstream of the sensor promoted a more even illumination of the sensor than would otherwise have been achieved, the half-width of the resulting electron-positron fluence distribution at the sensor plane was less than 0.5 cm. On the other hand, the aperture of the CC apparatus (to be described below) was of order 0.7 cm.. Thus, in order to ensure that the radiation dose was well understood over the region of exposure to the CC apparatus source, it was necessary to achieve a uniform illumination over a region of approximately 1 cm^2 . This was done by ‘rastering’ the detector across the beam spot through a range of 1 cm in both dimensions transverse to that of the incident beam. According to Monte Carlo simulation studies, this is expected to generate a region of approximately 1 cm^2 over which the illumination is uniform to within $\pm 20\%$. To account for potential millimeter-level misalignments of the beamline center with the sensor, a ‘targeting factor’ of $(90 \pm 10)\%$ is included in the final dose-rate calculations.

3. Dose Rates

During the 120 Hz operation of the SLAC Linear Collider Light Source (LCLS), 5-10 Hz of beam was deflected by a pulsed kicker magnet into the End Station

transfer line. The LCLS beam was very stable with respect to both current and energy. Electronic pickups and ion chambers measured the beam current and beam loss through the transfer line aperture, ensuring that good transfer efficiency could be established and maintained. The transfer efficiency was estimated to be $(95 \pm 5)\%$.

To calculate the dose rate through the sensor, it is necessary to determine the ‘shower conversion factor’ α that provides the mean fluence of minimum-ionizing particles (predominantly electrons and positrons), in particles per cm^2 , per incoming beam electron. This factor is dependent upon the radiator configuration and incident beam energy, as well as the rastering pattern used to provide an even fluence across the sensor (as stated above, the detector was translated continuously across the beam centerline in a 1 cm^2 square pattern).

To estimate α , the Electron-Gamma-Shower (EGS) Monte Carlo program [14] was used to simulate showers through the radiator configuration and into the sensor. The radiator configuration was input to the EGS program, and a mean fluence profile (particles per cm^2 through the sensor as a function of transverse distance from the nominal beam trajectory) was accumulated by simulating the showers of 1000 incident electrons of a given energy. To simulate the rastering process, the center of the simulated profile was then moved across the face of the sensor in 0.5mm steps, and an estimated mean fluence per incident electron as a function of position on the sensor (again, relative to the nominal beam trajectory) was calculated. This resulted in a mean fluence per incident electron that was uniform to within 20% 1mm anywhere inside the boundary of the rastering region. The value of α used for subsequent irradiation dose estimates was taken to be the value found at the intersection of the nominal beam trajectory with the sensor plane. The simulation was repeated for various values of the incident electron energy, producing the values of α shown in Tab. 3 (Tab. 4) for the 2013 (2014-15) radiator configuration. For years 2014 and 2015, the spacings of the radiator and sensor were close enough that a single mean value of α sufficed.

To convert this number to rads per nC of delivered charge, a mean energy loss in silicon of 3.7 MeV/cm was assumed, leading to a fluence-to-rad conversion factor of 160 rad per nC/cm^2 . It should be noted that while this dose rate considers only the contribution from electrons and positrons, these two sources dominate the overall energy absorbed by the sensor. In addition, the BeamCal dose-rate spec of 100 Mrad per year considered only the contribution from electrons and positrons.

To confirm the adequacy of the dose-calibration simulation, in 2013 an in-situ measurement of the dose

Table 3: Shower conversion factor α , giving the mean fluence at the sensor per incident electron, as a function of electron energy, for the 2013 radiator configuration. These values include the effect of rastering over a 1 cm^2 area surrounding the nominal beam trajectory. Also shown is the number of rads per nC of delivered charge, at the given energy, corresponding to the given value of α .

Beam Energy (GeV)	2013 Shower Conversion Factor α	Dose per nC Delivered Charge (krad)
2	2.1	0.34
4	9.4	1.50
6	16.5	2.64
8	23.5	3.76
10	30.2	4.83
12	36.8	5.89

was made using a radiation-sensing field-effect transistor (‘RADFET’) [15] positioned on a daughter board at the expected position of the nominal beam trajectory at the center of the rastering pattern. Beam was delivered in 150 pC pulses of 4.02 GeV electrons; a total of 1160 pulses were directed into the target over a period of four minutes, during which the sensor was rastered quickly through its 1 cm^2 pattern. The RADFET was then read out, indicating a total accumulated dose of 230 krad, with an uncertainty of roughly 10%. Making use of the dose rate calibration of Tab. 3, interpolating to the exact incident energy of 4.02 GeV, and taking into account the $(95 \pm 5)\%$ transfer efficiency of the ESTB beamline, leads to an expected dose of 250 krad, within the $\sim 10\%$ uncertainty of the RADFET measurement.

4. Sensor Irradiation Levels

Four types of silicon diode sensors were studied: p-type and n-type doped versions of both magnetic Czochralski and float-zone crystals. In what follows, we will use the notation ‘N’ (‘P’) for n-type (p-type) bulk sensors, and ‘F’ (‘C’) for float-zone (magnetic Czochralski) crystal technology. In addition, two GaAs sensors were irradiated. Once a sensor was irradiated with the ESTB, it was placed in a sub-freezing environment and not irradiated again. Up to four sensors of each type were irradiated and chilled until they could be brought back to the University of California, Santa Cruz campus for the post-irradiation CC and leakage current measurements. In addition, the sub-freezing environment was maintained both during and after the measurements, so that controlled annealing studies can eventually be done.

Table 4: Shower conversion factor α , giving the mean fluence at the sensor per incident electron, as a function of electron energy, for the 2014-15 radiator configuration. These values include the effect of rastering over a 1 cm^2 area surrounding the nominal beam trajectory. Also shown is the number of rads per nC of delivered charge, at the given energy, corresponding to the given value of α . For 2014 and 2015, the spacings of the radiator and sensor were close enough that a single mean value of α sufficed.

Beam Energy (GeV)	2014-15 Shower Conversion Factor α	Dose per nC Delivered Charge (krad)
3	4.6	0.73
5	10.0	1.60
7	15.5	2.48
9	21.1	3.38
11	26.7	4.27
13	31.8	5.09
15	37.7	6.03
17	43.0	6.88

Table 5 displays the dose parameters of the irradiated sensors. The $(95 \pm 5)\%$ transfer line efficiency and the $(90 \pm 10)\%$ targeting factor have been taken into account in these estimates. The numeral following the two letters in the sensor identifier refer to an arbitrary ordering of sensors assigned during the sensor selection. Sensors were held at between 0 and 5 C during irradiation. With the exception of sensor NC02, which was accidentally annealed for 5 hours at temperatures as high as 130 C, all sensors were transferred to a cold (below -10 C) environment immediately after irradiation. All four silicon diode sensor types were exposed to dose rates of approximately 5 and 20 Mrad, while an NF sensor received over 90 Mrad, an NC sensor 220 Mrad and a PF pad sensor 270 Mrad. Two GaAs sensors received doses of approximately 6 and 21 Mrad, respectively. CC and leakage current results for the irradiated sensors will be presented below.

5. Charge Collection Measurement

The SCIPP CC apparatus incorporates a ^{90}Sr source that has a secondary β -decay with an end-point energy of 2.28 MeV. These β particles illuminate the sensor under study, which is read out in one of two ways, depending upon whether it is a strip or pad sensor. These two charge collection readout approaches are described in detail below.

For strip sensors, 64 channels are read out by the PMFE ASIC [16], with a shaping time of 300 nsec.

Whenever one of the 64 channels exceeds a pre-set, adjustable threshold, the time and duration of the excursion over threshold is recorded. In addition, the $\sim 20 \text{ Hz}$ of β particles that pass through the sensor, and subsequently enter a small (2mm horizontal by 7mm vertical) slit, trigger a scintillator, and the time of excitation of the scintillator is also recorded. If the slit is properly aligned with the read-out channels of the sensor, and the sensor is efficient at the set read-out threshold, a temporal coincidence between the scintillator pulse and one of the read-out channels will be found in the data stream.

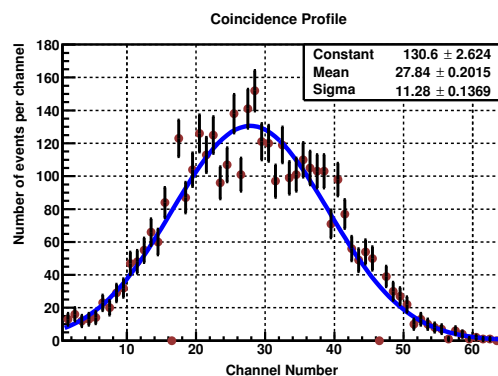


Figure 1: Sample profile of coincidences between the read-out sensor channels and the trigger scintillator. The integral of this distribution provides a count of the number of β particles triggering the scintillator that also exceeded the chosen PMFE threshold in one of the read-out channels.

Figure 1 shows a sample coincidence profile (histogram of the number of coincidences vs. channel number) for a strip sensor for a 150-second run at a given threshold and reverse bias level for one of the irradiated sensors (specifically, for the NC01 sensor after 5.1 Mrad of irradiation, applying a 300V reverse bias and a 130 mV threshold). The integral of the distribution yields an estimate of the total number of coincidences found during the run, which, when divided by the number of scintillator firings (after a small correction for cosmic background events) yields the median CC level at that threshold and bias level. This measurement can then be performed as a function of threshold level, yielding the curve shown in Fig. 2. For this plot, the abscissa has been converted from voltage (the applied threshold level) to fC (the PMFE input charge that will fire the threshold with exactly 50% efficiency) via a prior calibration step involving measurement of the PMFE response to known values of injected charge. The point at which the curve in Fig. 2 crosses the 50% level yields the median CC for the given bias level. In a prior study

of sensors irradiated with hadrons, the SCIPP apparatus gave median charge results consistent with that of other charge collection systems used to assess radiation damage in that study [17].

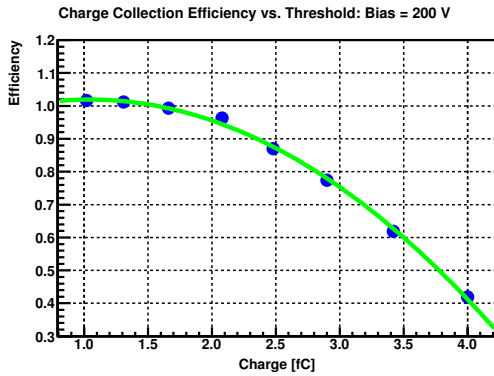


Figure 2: Plot of efficiency vs. PMFE threshold setting for one of the irradiated sensors. The abscissa has been converted from applied threshold voltage to the amount of input PMFE charge that will exceed the given threshold exactly 50% of the time. The point at which the curve crosses the 50% level yields the median CC for the given bias level.

For assessing the CCE of pad sensors, a two-stage, single-channel amplifier was constructed from discrete components, based on a design of Fabris, Madden and Yaver [18]. For the first stage, a cascode of two NXP BF862 JFETs is used. The source of the second JFET was connected to the non-inverting input of an LM6171 operational amplifier, chosen for its high slew rate and low input noise contribution. The output of this opamp was then fed back to the input of the first JFET, completing the negative feedback loop. An external network, including a 32 dB Sonoma Instrument 310 SDI amplifier, was used to further amplify the pulse and shape it to a rise-time of 290 ns.

Upon receiving a trigger from the scintillator, the signal from the amplifier was read out by a Tektronix DPO 4054 digital storage oscilloscope, and the digitized waveforms were written out and stored on the disk of a dedicated data-acquisition computer. After the waveforms were accumulated on the computer, a narrow temporal window was set around the peak of the average excitation pulse from through-going beta particles, and a histogram was made of the resulting pulse-height distribution; a typical distribution is shown in Fig. 3. Since not all β particles that trigger the scintillator go through the pad, the distribution shows contributions from both the Landau deposition of the through-going β particles, as well as that of the noise pedestal, allowing for an in-situ subtraction of the mean pedestal.

The amplification system was calibrated by reading out an unirradiated silicon diode sensor of known thickness, and comparing the median charge of the resulting Landau distribution (after subtracting off the mean pedestal) to that expected for an unirradiated sensor of that thickness. This yields a gain of approximately 40 mV/fC, with a small dependence on load capacitance. The width of the pedestal distribution then provides a measurement of the readout noise, which was found to be approximately 250 electrons at room temperature.

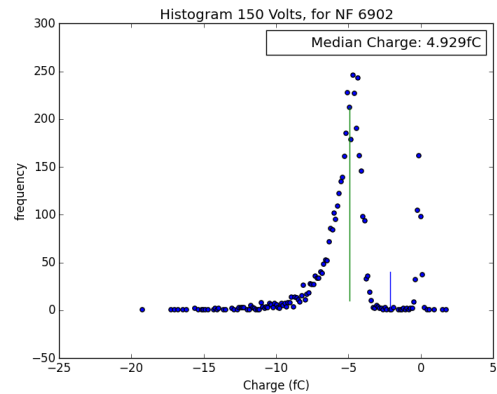


Figure 3: Histogram of pulse height for photomultiplier-triggered data events for the single-channel readout. Both the Landau distribution due to through-going β particles as well as the noise pedestal (for triggers for which the β particle did not traverse the sensor) are seen.

6. Charge Collection and Leakage Current Results

The daughter boards containing the irradiated sensors were designed with connectors that allowed them to be attached to the CC apparatus readout board without handling the sensors. The median CC was measured as a function of reverse bias voltage for each sensor both before and after irradiation.

A series of irradiation runs of between 5 and 220 Mrad was taken for the NC (n-type bulk magnetic Czochralski) sensor type. For the exposures of 5.1 (NC01) and 18.0 Mrad (NC10), no difference in CC performance was observed relative to the pre-irradiation studies of the NC01 and NC10 sensors. In Fig. 4 the median CC both before and after irradiation is plotted for the NC03 (90 Mrad dose) and NC02 (220 Mrad dose) sensors; it should be borne in mind, though, that the NC02 sensor experienced significant annealing before the post-irradiation measurement was done. It is seen that, while the depletion voltage increases significantly

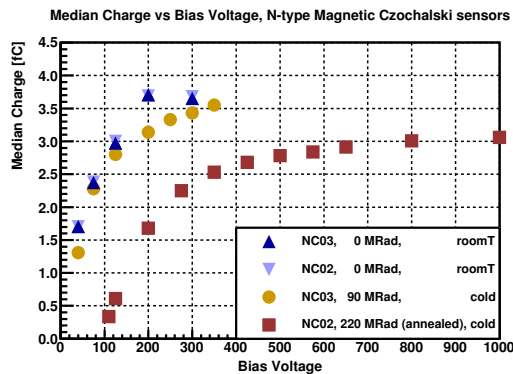


Figure 4: Median collected charge [fC] for the NC03 (90 Mrad dose) and NC02 (220 Mrad dose) sensors.

with dose, median CC within 20% of un-irradiated values is maintained for doses above 200 Mrad, although it may require annealing to maintain efficiency at that level.

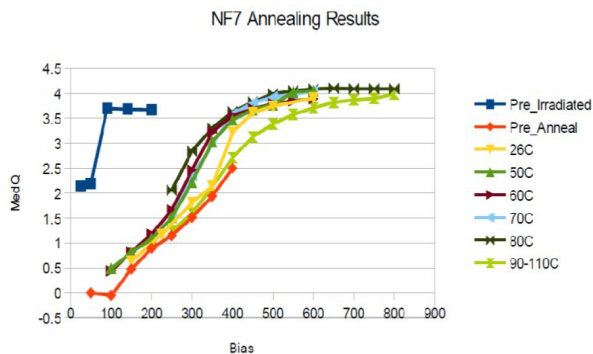


Figure 5: High-dose CC results for the NF07 (90 Mrad dose) sensor, as a function of annealing temperature. The sensor was annealed at the reported temperature for one hour.

A comprehensive study of the effects of annealing on CC was performed for an NF-type sensor after an exposure of 90 Mrad. Figure 5 exhibits the CC results for this sensor after annealing for one-hour periods over a series of progressively higher temperatures. After a one-hour annealing step at room temperature, full CC is observed for NF07 even after irradiation to nearly 100 Mrad, although the depletion voltage rose significantly with irradiation. The depletion voltage was observed to decrease significantly for annealing temperatures below 80° C (beneficial annealing), but then rose again for annealing temperatures in excess of 100° C (reverse annealing).

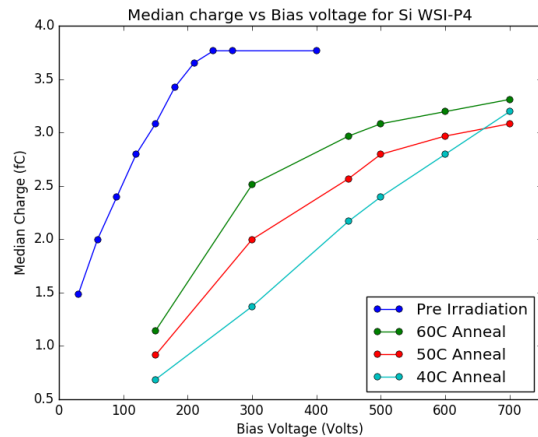


Figure 6: CC results for the WSI-P4 (PF pad) sensor before and after irradiation with a 270 Mrad dose, and after a series of annealing steps. Significant CCE remained after the 270 Mrad dose, with both the depletion voltage and CCE showing improvement with annealing at temperature of up to 60° C.

In 2015, a p-type float-zone pad sensor (WSI-P4) was irradiated to a total dose of 270 Mrad, and both leakage current and CCE were studied, both directly after irradiation as well as after one-hour annealing periods at successively higher temperature. Figure 6 shows the post-irradiation CCE (for 300 ns shaping time) as a function of bias voltage for the various stages of annealing. The CCE was seen to increase monotonically with bias voltage, reaching a maximum of approximately 85% of the pre-irradiation value above 600 V after a one-hour annealing period at 60° C.

Figure 7 shows the post-irradiation leakage current for sensor WSI-P4, measured at -10°C, as a function of bias voltage for the various stages of annealing. Relative to the pre-irradiation level of less than 10 nA, the current is seen to be significantly larger after irradiation, with little improvement observed as the sensor is annealed at successively higher temperature. At a bias voltage of 600 V the leakage current is observed to be about 2 μA, corresponding to a power draw of approximately 1.2 mW. Taking into account the 0.025 cm² area of the sensor, this corresponds to a post-irradiation power draw of approximately 50 mW/cm² after an exposure of 270 Mrad.

For the GaAs sensors, CCE and leakage current were measured both before and after exposures of 5.7 and 20.8 Mrad. Figure 8 shows the CCE as a function of bias voltage for the GaAs-18 sensor before and after a 5.7 Mrad irradiation, and then after an annealing step

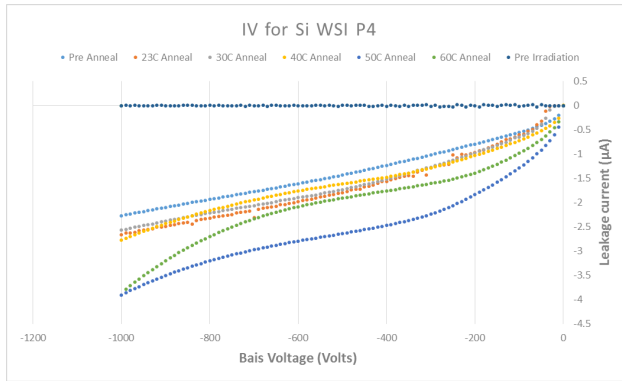


Figure 7: Leakage current at -10°C for the WSI-P4 p-type float-zone pad sensor after irradiation with a 270 Mrad dose, and after a series of annealing steps. Pre-irradiation leakage current was measured to be below 10 nA.

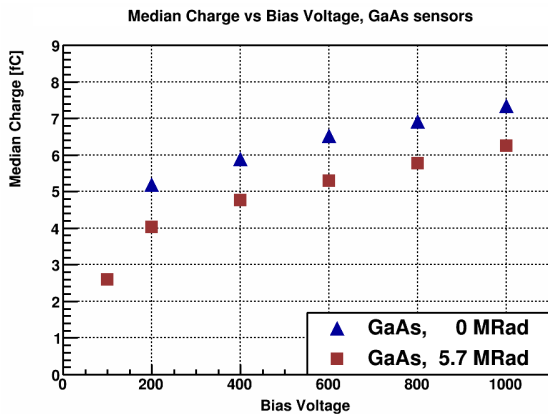


Figure 8: GaAs-18 sensor CCE before and after irradiation with a 5.7 Mrad dose.

for which the sensor was heated to 23°C for one hour. Since the GaAs sensor is not a diode, the CC does not reach a maximum as the applied voltage is raised. However, the CC is observed to drop by approximately 20% over the full range of applied voltage. This observation is roughly consistent with that of [12], which made use of an exposure of a pure beam of order-10-MeV electrons. Room-temperature annealing was seen to further degrade the CCE.

Figure 9 shows the CCE as a function of bias voltage for the GaAs-09 sensor before and after a 20.8 Mrad irradiation, and then after an annealing step at room temperature and at 30°C . Before annealing, but after irradiation, the CCE at a bias of 600 V was seen to decrease by over 40%; after annealing at 30°C , the CCE was further reduced to a level of approximately 15% of its pre-

irradiated value. Again, this CCE loss after 21 Mrad of exposure is consistent with that of [12].

Figure 10 shows the post-irradiation leakage current for GaAs-09 (20.8 mRad exposure), measured at -10°C , as a function of bias voltage for the various stages of annealing. Relative to the pre-irradiation level of less than 10 nA, the current at a bias voltage of 600 V is seen to rise to a fraction of a microamp after irradiation, leading to leakage currents of less than $1\ \mu\text{A}/\text{cm}^2$ over the $0.21\ \text{cm}^2$ area of the GaAs pad sensors. Annealing is seen to markedly reduce the post-irradiation leakage current, although as discussed above, the same annealing steps dramatically reduced the CCE.

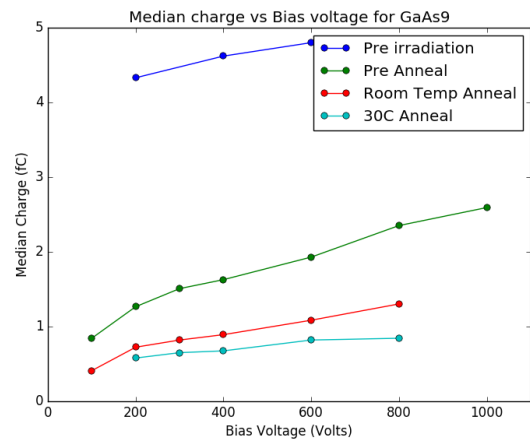


Figure 9: CCE results for the GaAs-09 sensor before and after irradiation with a 20.8 Mrad dose, and after a series of annealing steps. CCE was observed to degrade substantially with irradiation, and degrade further with annealing.

Table 6 provides a table of maximum median collected charge, both before and after irradiation, and median charge loss due to irradiation, for all sensors studied.

7. Summary and Conclusions

We have explored the radiation tolerance of four different types of silicon diode sensors (n-type and p-type float zone and magnetic Czochralski bulk) sensors, as well as a GaAs sensor, exposing them to doses as high as 270 Mrad at the approximate maxima of tungsten-induced electromagnetic showers. For the two types of silicon diode sensors (n-type Czochralski and p-type float zone) explored with several-hundred Mrad doses, we have found charge-collection efficiency in excess of 80% for a bias voltage of 600 V. For the p-type float

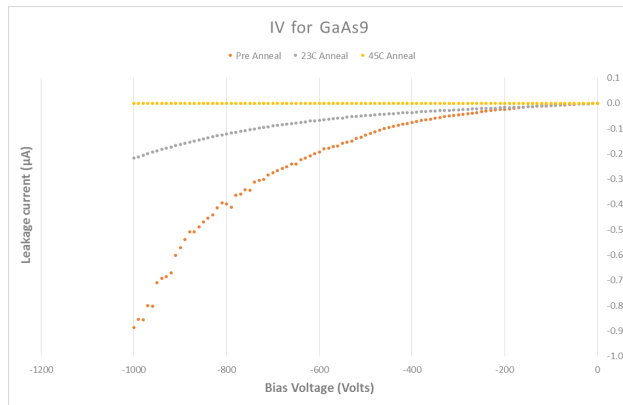


Figure 10: Leakage current at -10° C for the GaAs-09 sensor after irradiation with a 20.8 Mrad dose, and after a series of annealing steps. Pre-irradiation leakage current was measured to be below 10 nA.

zone sensor after irradiation with 270 Mrad, the leakage current at a temperature of -10° C was measured to be approximately $80 \mu\text{A}/\text{cm}^2$. This suggests that, with the application of active cooling, silicon diode sensors may be sufficient for the operation of a calorimeter exposed to hundreds of Mrad, approaching the specification required for the most heavily irradiated sensors in the ILC BeamCal instrument. While the depletion voltage increases significantly with radiation, studies of the charge-collection efficiency as a function of annealing temperature suggests that the depletion voltage can be significantly decreased after one-hour annealing runs at temperatures up to 80° C. On the other hand, the GaAs sensors showed significant loss of charge-collection efficiency even for modest radiation doses of 6 Mrad; for a dose of 21 Mrad the charge-collection efficiency was reduced by nearly 60%. Room-temperature annealing further reduced the charge-collection efficiency to 17% of the value measured before irradiation. In all cases, however, the leakage current remained below $1 \mu\text{A}/\text{cm}^2$.

In the most recent run of experiment T-506, a full complement of n- and p-type float zone and magnetic Czochralski pad sensors were exposed to doses of approximately 300 Mrad each. For the case of the p-type float zone sensor, which had already been irradiated and studied as discussed above, the total accumulated dose is now approaching 600 Mrad. In addition, a silicon carbide sensor was exposed to a dose of 100 Mrad. The CCE and leakage current performance of these sensors is currently under evaluation.

8. Acknowledgments

We are grateful to Leszek Zawiejski, INP, Krakow for supplying us with the tungsten plates needed to form our radiator, and Georgy Shelkov, JINR, Dubna for supplying us with GaAs sensors for irradiation studies. We would also like to express our gratitude to the SLAC Laboratory, and particularly the End Station Test Beam delivery and support personnel, who made the run possible and successful. Finally, we would like to thank our SCIPP colleague Hartmut Sadrozinski for the numerous helpful discussions and guidance he provided us.

9. Role of the Funding Source

The work described in this article was supported by the United States Department of Energy, DOE contract DE-AC02-7600515 (SLAC) and grant DE-FG02-04ER41286 (UCSC/SCIPP). The funding agency played no role in the design, execution, interpretation, or documentation of the work described herein.

References

- [1] Y. Unno et al, *Development of n-on-p silicon sensors for very high radiation environments*, NIM A 636, S24 (2011).
- [2] ILD Concept Group, *International Large Detector DBD*, <http://www.linearcollider.org/ILC/physics-detectors/Detectors/Detailed-Baseline-Design>, Chapter 4 (2012).
- [3] SID Collaboration, *SiD Detailed Baseline Design*, <http://www.linearcollider.org/ILC/physics-detectors/Detectors/Detailed-Baseline-Design>, Chapter 5 (2013).
- [4] J.R. Carter and R.G. Downing, 'Charged Particle Radiation Damage in Semiconductors: Effect of Low Energy Protons and High Energy Electrons on Silicon', Interim Technical Final Report, TRW Apce Technology Laboratories, May 1965.
- [5] T. Noguchi and M. Uesugi, 'Electron Energy Dependence of Relative Damage Coefficients of Silicon Solar Cells for Space Use', Technical Design of the International PVSEC-5, Kyoto, Japan (1990).
- [6] Geoffrey P. Summers et al., 'Damage Correlations in Semiconductors Exposed to Gamma, Electron, and Proton Radiations', IEEE Transactions on Nuclear Science 40, 1372 (1993).
- [7] J.M. Rafi et al., 'Degradation of High-Resistivity Float Zone and Magnetic Czochralski n-type Silicon Detectors Subjected to 2-MeV Electron Irradiation', NIM A 604, 258 (2009).
- [8] S. Dittongo et al., 'Radiation Hardness of Different Silicon Materials after High-Energy Electron Irradiation', NIM A 530, 110 (2004).
- [9] S. Dittongo et al., 'Studies of Bulk Damage Induced in Different Silicon Materials by 900 MeV Electron Irradiation', NIM A 546, 300 (2005).
- [10] G. Casse et al., 'First Results on Charge Collection Efficiency of Heavily Irradiated Microstrip Sensors Fabricated on Oxygenated p-type Silicon', NIM A 518, 340 (2004).
- [11] G. Casse, 'Radiation Hardness of p-type Silicon Detectors', NIM A 612, 464 (2010).
- [12] K. Afanaciev et al., 'Investigation of the radiation hardness of GaAs sensors in an electron beam', JINST 7, P11022 (2012).

- [13] R. Band *et al.*, 'Initial results of a silicon sensor irradiation study for ILC extreme forward calorimetry', NIM A 765, 41-16 (2014).
- [14] The Electron Gamma Shower (EGS) Monte Carlo Program, <http://rcwww.kek.jp/research/egs/>.
- [15] The specific device used was the REM Oxford Ltd. corporation's REM TOT601B device, <http://www.radfet.com/index.html>.
- [16] Hartmut F.-W. Sadrozinski *et al.*, 'The Particle Tracking Silicon Microscope PTSM', IEEE Transactions on Nuclear Science 51, 2032 (2004).
- [17] K. Hara *et al.*, 'Testing of bulk radiation damage of n-in-p silicon sensors for very high radiation environments', NIM A 636, S83 (2011).
- [18] L. Fabris, N. W. Madden and H. Yaver, 'A fast, compact solution for low noise charge preamplifiers', NIM A 424, 545-551 (1999).

Table 5: Dose parameters of the irradiated sensors. A $(95 \pm 5)\%$ transfer line efficiency and a $(90 \pm 10)\%$ targeting factor has been taken into account in final dose estimates. While the NC02 sensor was irradiated at a temperature of 5 C, it was accidentally annealed for approximately 5 hours at temperatures as high as 130 C.

Sensor	Strip (S) or Pad (P)	Year 2013	Beam Energy (GeV)	Delivered Charge (μC)	Dose (Mrad)
PF05	S	2013	5.88	2.00	5.1
PF14	S	2013	3.48	16.4	19.7
PC10	S	2013	5.88	1.99	5.1
PC08	S	2013	(5.88, 4.11, 4.18)	(3.82,3.33,3.29)	20.3
NF01	S	2013	4.18	2.30	3.7
NF02	S	2013	4.02	12.6	19.0
NF07	S	2013	8.20	23.6	91.4
NC01	S	2013	5.88	2.00	5.1
NC10	S	2013	3.48	15.1	18.0
NC03	S	2013	4.01	59.9	90.2
NC02	S	2013	(10.60,8.20)	(32.3,13.8)	220
GaAs-18	P	2014	3.87	6.03	5.7
GaAs-09	P	2014	3.90	21.7	20.8
WSI-P4 (PF)	P	2015	13.32	50.9	269

Table 6: Maximum median CCE before and after irradiation. While the NC02 sensor was irradiated at a temperature of 5^o C, it was accidentally annealed for approximately 5 hours at temperatures as high as 130 C. Room-temperature annealing was required to recover the full CC for the NF07 sensor. For the WSI-P4 sensor (PF pad sensor), the quoted charge CCE is that after annealing at 60^o C For the GaAs sensors, the quoted CCE is that before the sensor spent a significant amount of time above -10^o C; annealing was found to significantly degrade the CCE for GaAs sensors.

Sensor	Dose (Mrad)	Median CC Before Irradiation (fC)	Median CC After Irradiation (fC)	Fractional Loss (%)
PF05	5.1	3.70	3.43	7
PF14	20	3.68	3.01	18
PC08	20	3.51	3.09	12
NF01	3.7	3.76	3.81	0
NF02	19	3.75	3.60	4
NF07	91	3.75	4.00	0
NC01	5.1	3.71	3.80	0
NC10	18	3.76	3.74	1
NC03	90	3.68	3.55	4
NC02	220	3.69	3.06	17
WSI-P4 (PF) (@600 V)	269	3.77	3.17	16
GaAs18 (@600 V)	5.7	6.41	5.22	19
GaAs09 (@600 V)	20.8	4.74	2.02	57